Available online at www.sciencedirect.com
SCIENCE DIRECT®
Journal of volcanology and geothermal research
ELSEVIER
Journal of Volcanology and Geothermal Research 123 (2003) 161–180
www.elsevier.com/locate/jvolgeores

Digital photogrammetry as a tool in analogue modelling: applications to volcano instability

F. Donnadieu *, K. Kelfoun, B. van Wyk de Vries, E. Cecchi, O. Merle

Laboratoire Magmas et Volcans, Observatoire de Physique du Globe de Clermont-Ferrand, Université Blaise Pascal – CNRS, 5 rue Kessler, 63038 Clermont-Ferrand, France

Received 7 August 2001; received in revised form 21 December 2001; accepted 29 January 2002

Abstract

Three techniques of digital photogrammetry have been applied successfully to laboratory analogue models to study surface displacements caused by various volcano deformation types. Firstly, side-perspective videos are used to differentiate profile displacements between cryptodome intrusion models and models deforming by ductile inner-core viscous flow. Both models show similar morphologic features including a bulged flank and an asymmetric upper graben. However, differences in displacement trajectories of the bulge crest reflect upward intrusion push contrasting with essentially downward displacement vectors of weak core models. The other two techniques use vertical views correlated automatically either as time-sequence monoscopic views or as coeval stereoscopic pairs. This exploits to a maximum the method's potential by imaging surface displacements over the whole model. Successive monoscopic photograms, because they suffer only moderate numerical processing for topographic effect removal, can detect very small displacements occurring early in deformation processes. As illustrated by analysis of intrusion models, the monoscopic method allows prediction of fault locations and main displacement locations. It can also anticipate the principal strain directions, and separate different deformation stages. On the other hand, the stereo-photogrammetry technique, although more complicated, provides topography and volume changes, as well as pictures of surface displacements in three dimensions. Results are presented for the spreading of volcano models on a ductile substratum and viscous cored cones. We have found digital photogrammetry to be a useful tool for analogue modelling, because it provides quantitative data on surface displacements, including movement invisible to the eye, as well as topographic changes. It is a good method for investigating and comparing different deformation mechanisms. It is especially useful for interpretation of displacement patterns obtained from monitoring of natural active volcanoes. In fact, results of the methods used in the laboratory can be directly compared with field data from geodetic or photogrammetric surveys, as at Mount St. Helens in 1980.

Keywords: analogue model; digital photogrammetry; stereo-photogrammetry; volcano instability; displacement; slope stability

1. Introduction

The growth of volcanoes is characterised by episodes of instability that can lead to structural deformation and flank failure turning to a debris

* Corresponding author. Tel.: +33-4-73-34-67-65; Fax: +33-4-73-34-67-44.
E-mail address: f.donnadieu@opgc.univ-bpclermont.fr (F. Donnadieu).

0377-0273/03/$ – see front matter © 2003 Elsevier Science B.V. All rights reserved.
doi:10.1016/S0377-0273(03)00034-9

avalanche. Instability may occur in response to one or a combination of different possible factors (see Borgia et al., 2000 for a review). These include slope steepening (e.g. Siebert, 1984; Begét and Kienle, 1992), flank overloading by the accumulation of eruptive products (e.g. Murray, 1988), magma intrusion (e.g. Gorshkov, 1959; Moore and Albee, 1981; Lipman et al., 1981; Voight et al., 1981; Siebert et al., 1987; Elsworth and Voight, 1995; Voight and Elsworth, 1997; Voight, 2000; Donnadieu et al., 2001), mechanical weakening due to hydrothermal activity (e.g. Lopez and Williams, 1993; Day, 1996), increase in pore fluid pressure (e.g. Elsworth and Voight, 1996; Voight and Elsworth, 1997), seismicity (e.g. Kanamori et al., 1984; Siebert, 1984), tectonic movement (e.g. Francis and Self, 1987; Carracedo, 1994; Tibaldi, 1995), gravitational spreading (e.g. Borgia, 1994; Merle and Borgia, 1996; van Wyk de Vries and Francis, 1997; van Wyk de Vries and Matela, 1998), or undermining effects of peripheral erosion (e.g. Guest et al., 1988; Moore and Clague, 1992; Firth et al., 1996). Volcano instability can develop over various time scales from months to hundreds of years and involve volumes varying over several orders of magnitude up to several thousands of cubic kilometres (McGuire, 1996).

Since the pioneer work of Cloos (1928), analogue modelling has been widely used to investigate deformation mechanisms and structures associated with tectonic processes (cf. McClay, 1996) and salt tectonics (e.g. Weijermars et al., 1993). For over a century, many experimental studies have also been dedicated to deep magmatic intrusions into crustal country rocks (e.g. Howe, 1901; Ramberg, 1970, 1981), dike emplacement (e.g. Fiske and Jackson, 1972; Pollard and Johnson, 1973), or superficial intrusions in a sedimentary cover (Merle and Vendeville, 1995; Roman-Berdiel et al., 1995, 1997; Benn et al., 1998). More recently, scaled models have been designed to study various processes leading to volcano instability, including gravity spreading (Merle and Borgia, 1996; van Wyk de Vries and Matela, 1998; van Wyk de Vries et al., 2000), regional tectonics (Tibaldi, 1995; van Wyk de Vries and Merle, 1996, 1998; Lagmay et al., 2000; Vidal and Merle, 2000; Merle et al., 2001), caldera formation (Komuro et al., 1984; Komuro, 1987; Martí et al., 1994; Roche et al., 2000; Acocella et al., 2000; Lagabrielle et al., 2001), superficial intrusions (Donnadieu and Merle, 1998, 2001; Lagmay et al., 2000), and domes (e.g. Blake, 1990; Fink and Griffiths, 1990, 1998). Most of these studies use surface photography to map structures and sections cut through models to characterise internal deformation.

Surface displacements of real volcanic edifices are often large and rapid enough to be monitored, as illustrated by the intrusion-induced bulging of the northern flank of Mount St. Helens in March–May 1980. Geodetic (Lipman et al., 1981) and photogrammetric (Moore and Albee, 1981; Jordan and Kieffer, 1981) records revealed a northward displacement of the bulge centre of about 150 m ascribed to the growth of the 114×10^6 m^3 magmatic cryptodome over 2 months. Comparison to model displacements can help interpret and bring constraints on the mechanical processes operating at depth provided models are properly scaled, according to the theory of Hubbert (1937) for geometric, dynamic, and kinematic scaling, and as shown by Donnadieu and Merle (2001) in the particular case of the Mount St. Helens intrusion. This is a major concern for volcano instability because cumulative displacement may lead to a catastrophic destabilisation of the flank (Voight, 1988). The presence of magma may dramatically enhance the explosive capacity that represents an additional hazard to the devastating landslide (Alidibirov and Dingwell, 1996). In order to compare the deformation of natural volcanoes with that in the scaled models where the source mechanism is known, an accurate way of measuring model displacements is needed. In most experimental studies, however, classical qualitative photographic analysis is used to describe model displacements of a number of discrete points.

We present here an application of three photogrammetric techniques to analogue models of volcano deformation. We show that digital photogrammetry, in a broad sense, is a powerful tool in analogue modelling. It provides useful quanti-

tative data on surface displacements that allow the interpretation of laboratory model deformation processes. It can give advance prediction, through the detection of very small displacements, of the location of developing structures. Case examples illustrate the brittle deformation of volcanic edifices produced by viscous intrusions, by viscous flow of a weak inner core and by gravity spreading on a ductile substratum. This approach can also be used in real situations, assuming that the deformation rates and magnitudes are large enough to be detected by photography at a distance.

2. Principles of digital photogrammetry

A basic and very general definition of photogrammetry would be a technique devoted to determine dimensions of objects by means of measurements made from perspective views, usually photographs, of these objects. Photographs of a given object can be compared to obtain surface displacement data if they are taken from the same spot at successive instants in time, i.e. monoscopic views. Also, photographs taken in a short interval of time from different spots and showing the same surface part of an object can be used to calculate the object topography in three dimensions, i.e. a digital elevation model (DEM). Time-successive DEMs, in turn, can be compared to compute topographic changes, volume changes, and 3-D views of displacements for each pixel area or selected points.

The term digital photogrammetry is often used in reference to work done from a stereoscopic pair of aerial photographs. Hereafter, we use this term in a broader sense, including stereoscopic and monoscopic digitised images taken vertically above, or from the side of, the model and that have been processed numerically to obtain quantitative information. Classical or digital photogrammetric methods have been applied for years to natural volcanoes of Earth and other planets (e.g. Moore and Albee, 1981; Jordan and Kieffer, 1981; Fink et al., 1990; Zlotnicki et al., 1990; Head, 1996; Mattioli et al., 1996; Maciejak, 1998; Kelfoun, 1999; Yamashina et al., 1999; Baldi et al., 2000) or to mountain-slope instabilities (e.g. Weber and Hermann, 2000) in order to get spatio-temporal data, either displacement data or topographic and volume data, as well as to facilitate mapping.

Photograph correlations, once hand-made, can now be conveniently made from two digitised images by automatic numerical processing, allowing information to be obtained for a continuous surface area. The automatic correlation that we used works with the region-growing algorithm of Otto and Chau (1989). It is based on the adaptative least-squares correlation technique developed by Gruen (1985). The advantages of doing this numerically are several-fold: (1) a better accuracy for matching points and ensuing displacement or volume computations; (2) less time-consuming; (3) resulting data for the entire area covered by both images; (4) easy plotting of results.

Unlike natural volcanoes in the field, the laboratory conditions are ideal for the application of such a method because they do not suffer from weather whims and also because the camera settings can be chosen to avoid too many numerical corrections, and prepared meticulously in advance. The accuracy of the results depends upon the resolution of photographs used, the experimental setting conditions, and upon the resolution chosen for the computation of the DEM (the higher the resolution, the higher the noise). Although weather presents a problem in photography of real volcanoes, alternative deformation-monitoring techniques such as InSAR are also limited by the repeat interval due to satellite orbit parameters, and so one advantage of photogrammetry is that it can be used to monitor more rapid and immediately threatening deformations than can InSAR. Furthermore, one of the benefits of using standard aerial photography equipment and settings is that routine aerial photographic surveys can be carried out as a pre-eruption or pre-unrest baseline with which repeated photographs can be compared. Note also that there are safety advantages, at least until an eruption column is present and may threaten aircraft, of using aerial photography-based techniques relative to ground-based deformation monitoring (classical geodetic, laser-ranging and GPS geodetic).

3. Summary of experiments

We have used photogrammetric techniques to analyse three series of experiments reproducing deformation features observed on real volcanoes and that we summarise here.

3.1. Flank bulging by intrusion

Flank bulging due to the viscous magma intrusion has been observed at Bezymianny volcano in 1956 (Gorshkov, 1959), Mount St. Helens in 1980 (e.g. Voight et al., 1981), or Usu-Shinzan volcano in 1978–1983 (Katsui et al., 1985). The first two cases led to a voluminous sector collapse because the edifices were steep-sided, whereas Usu-Shinzan did not collapse because the magma intruded nearly flat-ground.

We have recently carried out scaled analogue modelling of viscous cryptodome intrusion into volcanic cones (Donnadieu and Merle, 1998). Silicone putty, the magma analogue, was injected vertically at the base of a cohesive cone made up of sand and flour. Models always show the same deformation mechanism, called viscous indentation. Typically, a major shear fault, which propagates initially from one side of the intrusion to the opposite flank, was found to guide the intrusion obliquely. It causes one flank to bulge outward in the footwall region and then an asymmetric graben to form in the hanging-wall region near the cone summit. The outward motion of the bulge is further accommodated by the curving of the major shear fault into tear faults bounding the bulge laterally and eventually merging together to form a thrust fault at the base of the bulge (Merle and Donnadieu, 2000). The accompanying internal structures can significantly reduce the stability of the deformed steep flank and may lead to its destabilisation, as at Bezymianny and Mount St. Helens (Donnadieu et al., 2001).

3.2. Flank slumping by gravitational deformation

A similar bulge morphology exists on the flank of Casita volcano, Nicaragua, without associated eruptive activity (van Wyk de Vries et al., 2000; Kerle and van Wyk de Vries, 2001). On the basis of analogue models as well as structural and morphologic evidence, the authors interpret these features as the result of slow creep of the hydrothermally altered volcano core. Therefore, it turns out that similar topographic features in the field may result from different deformation processes. Note, however, that flank bulging due to an intrusion involves an increase in volume of the volcanic edifice, whereas flank slumping inferred to result from gravitational deformation is a constant-volume process.

Models with scaling parameters similar to those of van Wyk de Vries et al. (2000) were compared with the above intrusion experiments. In the ductile core models, a spherical inclusion of silicone was buried in a cohesive cone, and offset from the cone centre, to simulate slope changes and fault patterns in a weak-cored edifice. Varying the volume and geometry of the silicone inclusion did not change the resulting structures significantly, although a volume increase raised the deformation rates. The cone summit, initially 10 cm high, first flattened above the silicone and was bounded by horseshoe-shaped normal faults. An area of localised flank steepening then occurred by the side of the silicone inclusion and was later fronted by thrust faults downhill. The slump-like structures therefore lead to a convex–concave morphology of the flank.

3.3. Models of volcano spreading

Many examples of volcano spreading have been recognised worldwide as well as on extraterrestrial edifices (Borgia et al., 1992, 2000; Merle and Borgia, 1996; van Wyk de Vries and Francis, 1997; van Wyk de Vries et al., 2000). Scaled analogue models of radial spreading like those of Merle and Borgia (1996) have been used for photogrammetric analysis. A slightly cohesive cone, 10 cm high, made up of sand and flour, was built on a ductile substratum made up of a basal layer of viscous silicone (1–2 cm thick), simulating weak strata (e.g. sediments), overlaid by a layer of sand (1 cm thick). The silicone spread radially under the load of the cone away from the centre. Major normal faults and their conjugates formed leaf grabens with an overall radial direction and ac-

commodated the concentric extension, while other, minor, non-radial faults accommodated internal deformation of the cone due to its sagging. The leaf grabens intersected in the central region of the cone, producing on top a flat circular area. A shield morphology progressively developed as the cone diameter increased and the edifice height decreased. Outward motion of the flanks caused peripheral compression expressed at the surface by a concentric ridge of fault-propagation anticlines or thrust faults verging away from the cone (cf. Merle and Borgia, 1996).

4. Side-perspective videos

4.1. General features

The most simple but efficient technique we used is side-perspective videos. Pictures are extracted at selected time intervals from side-perspective video films of the experiments, and then digitised using a standard video-play software. The technique is designed to obtain quickly profiles of displacement trajectories in two dimensions from a few selected discrete points at the surface of a model. As data are not required for a continuous surface area, comparison of a point's position on successive photographs can be done manually and there is no need to use the automatic correlation process in this case. Typically, the chosen points lay on the line of greatest displacements or in a zone where the user may expect specific displacements.

4.2. Experimental setting

We used a CCD-VX1E Hi8 camcorder providing high quality images with 410 000 pixels each. The video camera was placed at a distance where the model matched the full size of the screen, usually at 60–90 cm. In these conditions, each picture represented a zone of about 10×15 cm of the model, leading to a pixel resolution of much less than 0.1 mm. The camera's focal axis must be as close as possible to the normal of the displacement plane, i.e. horizontal in our case and at the same level as the model centre (Fig. 1a). Measurements of vertical displacements were made in the vertical displacement plane, thus requiring no correction. In order to be able to see the cone profile along the line of largest displacements, the camera had to be placed at an angle slightly less than 90° from the deformation axis. Therefore, the real horizontal displacements (x_{real}) were viewed at an angle α from the displacement plane and the ensuing effect on the measured displacements (x_{measured}) can be calculated from:

$$x_{\text{real}} = \frac{x_{\text{measured}}}{\cos\alpha}$$

As α typically ranges from 5° to 10°, the error represents less than 1.5% of the measured value and can be neglected.

A scale object was placed in the vertical plane of motion in order to provide an absolute scale for displacement vectors during the image processing as well as for comparison purposes with other experiments. Black grains of silicon carbide, about 1 mm in diameter, were poured onto the model surface to provide tracers to follow reference points. This provided the resulting images with good contrast and texture, as most models were built with a light-coloured cohesive mix of sand and flour. Digitised images were compared using image viewing software by superimposing immobile reference points common to all pictures. The displacements of selected points on the model outline were then determined from the offset with previous pictures.

The accuracy of the displacement measurements depends upon the size of the model on the image, the resolution used to digitise the images and the quality of the video camera and the videotape. In our experiments, the displacement detection threshold was less than 0.1 mm.

4.3. Side-perspective analysis

Photogrammetric analyses have been carried out on both types of analogue models using the side-perspective video technique to follow the trajectories of points on the line of greatest displacement. Outward radial displacements in the two types of model are surprisingly similar (Fig. 1). Both display two distinct displacement areas: (i) upslope of the topographic peak, linear subsidence occurs in the asymmetric graben with an

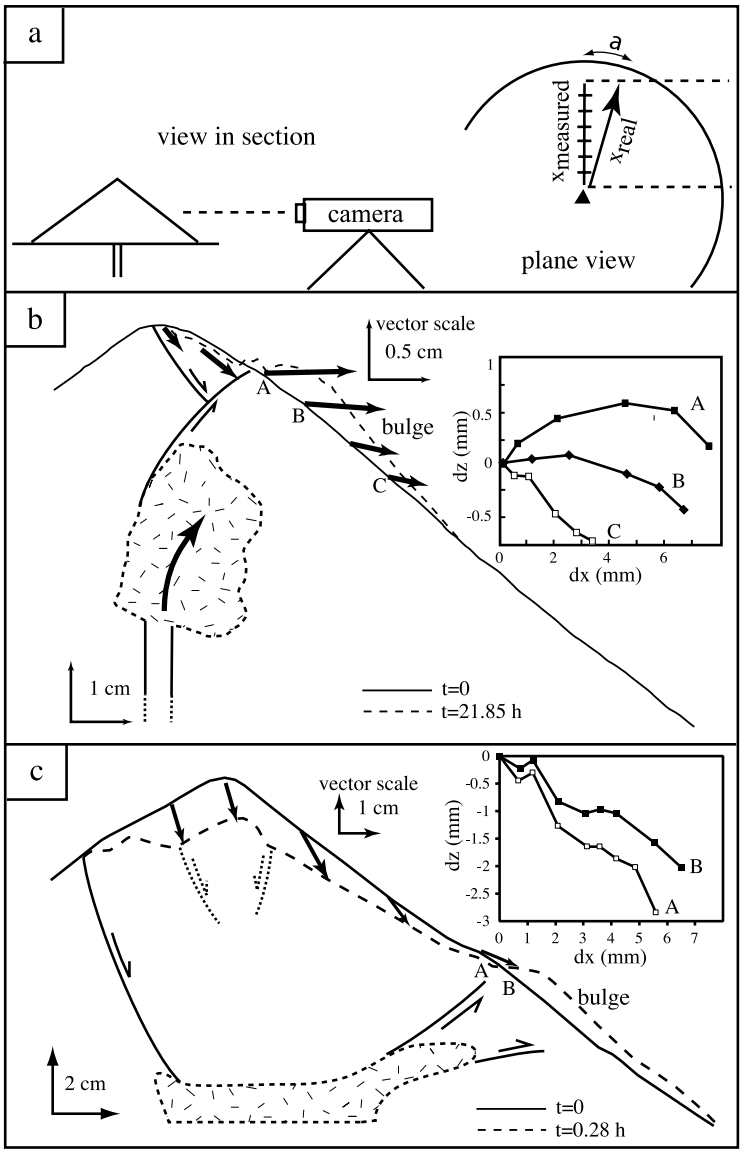

Fig. 1. Results of the side-perspective video technique applied to two models. (a) Experimental apparatus in side and plan views. (b) Vertical intrusion model simulating cryptodome emplacement after 21.85 h. Injection velocity was 1.72 cm/h, conduit diameter 0.4 cm, initial cone height 7.4 cm and injection level 3 cm. (c) Volcanic cone models with ductile core (silicone) simulating hydrothermally altered inner part after 20 min. The silicone inclusion was not centred (2 cm offset), had initial radius of 3 cm and 4 cm height; the cone's initial height was about 10 cm. Note the lateral bulge and summit graben structures in both cases and the different displacement patterns on the bulge for both models.

outward angle which mimics the dip of the main horseshoe fault; (ii) downslope of the topographic peak, displacement vectors are slightly inclined downward, decreasing in magnitude downhill from the bulge crest. Although these structures appear to be wider for the soft-core models in Fig. 1, their extent can vary with the size of the silicone inclusion and its initial depth (Cecchi et al., 2001). Therefore, the discrimination of the type of deformation mechanism, i.e. hydrothermal

weakening or intrusion, must be made from the flank-profile displacement patterns.

Although most bulge displacement vectors have a slight downward component, points on the upper part of the bulge clearly show an upwards-then-downwards trajectory. This upward evolution of the crest points is observed at the very beginning of the deformation in the intrusion models. It is thought to reflect directly the upward intrusion push at the footwall of the oblique major shear fault, whereas points of the flank located under the intrusion front level are simply pushed aside (Fig. 1b). The graben represents a smaller area collapsing passively as the flank is pushed aside. As this is an increasing-volume deformation process, the bulge volume coarsely represents the collapse volume of the graben plus the additional volume of the intrusion. At the crest of the bulge, one can therefore expect displacements larger than those obtained in the case of a constant-volume process (other parameters being equal) as well as displacements with a strong and long-lasting upward vertical component. The bulge-point trajectory profiles are very similar to those recorded by geodetic monitoring at Mount St. Helens when a cryptodome intruded the north flank in May 1980 (Lipman et al., 1981; Fig. 2a).

In the case of the soft-cored cones, deformation occurs at constant volume so that the volume of the bulge equals that of the graben. The volume loss of the cone through initial graben collapse is progressively counterbalanced by flank bulging. This is produced by the lateral escape of the silicone pushing the lower part of the flank along gently dipping faults that preclude strong and sustained vertical displacements. Surface point trajectories of volcano models with a ductile core show outward displacements with a much stronger downward component (Fig. 1c). On the upper part of the bulge, points initially show a downward trajectory, followed later on by a low-amplitude up-and-down trajectory, unlike points of the bulge in the intrusion models. The initial collapse corresponds to the sagging of the upper cone into the silicone, which is flattening at first. The following tiny upward component is caused by the core being pushed outwards and slightly upwards in the weakest flank, i.e. in the direction of the silicone inclusion offset to the centre. This causes asymmetrical collapse to impinge on the weak flank.

4.4. Comparison between ductile core and intrusion models

The deformation patterns are similar in both types of models but the technique used here to retrieve displacement profiles reveals some differences. In addition to the timing of the upwards-then-downwards trajectory, there is also a more gradual transition between the displacement pattern of the graben and that of the bulge in the case of the soft-core models. In the intrusion models the limit is sharper, marked by a topographic peak that represents the emergence of a steeply inward-dipping shear fault and that is easily recognised in the field. Another major difference in the two models is strain rate. The intrusion models generally take several hours to complete, with a reasonable injection rate (0.1–4 cm^3/h), and represent a natural deformation of days–months to a few years with magma viscosities of the order of 10^{11} Pa s. This corresponds to an average displacement rate of the order of 1 m per day or month to reach 100–150 m outward displacement, assuming that the bulged flank would collapse beyond this limit because of large strain and strain rate inducing the rock strength weakening. In contrast, the soft-core models take about 30 min to complete and simulate hydrothermalised rocks with a viscosity of the order of 10^{18} Pa s flowing over a time scale of thousands to hundreds of thousands of years. To reach a displacement of about 100 m, an average displacement rate closer to 1 m per thousand years is needed. From this it follows that, normally, the indentation process is much more rapid than the soft-core deformation, and would normally not be confused in the field, except where no deformation data are available.

We do not know, however, the real viscosity of an altered core under high fluid pressures, nor the real range of intrusion rates possible. Thus, we cannot discount the possibility that gravity spreading may deform at rates approaching intru-

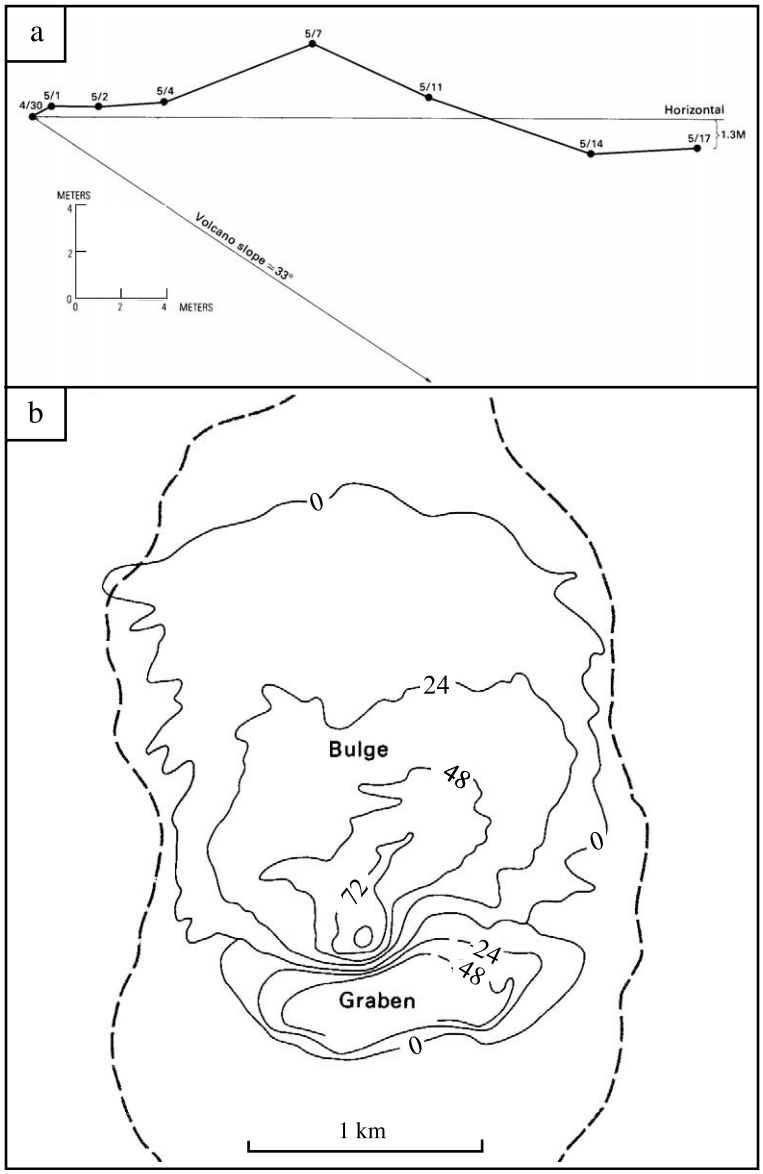

Fig. 2. Deformation of Mount St. Helens during the cryptodome intrusion in 1980. (a) Displacements measured at the crest of the bulge from April 30 to May 17 (Lipman et al., 1981). (b) Elevation changes in meters on April 7, 1980. Dashed line: limit of May 18 crater (Moore and Albee, 1981).

sion under some circumstances. Indeed, once an intrusion is emplaced, and if it is large enough to overcome cooling effects, it is likely to deform by spreading. Moreover, rate of deformation (i.e. quantitative kinematic) criteria might not always be useful in distinguishing intrusion-driven from alteration weakening- or pore-fluid pressurisation-driven cases. Certain collapses (e.g. Unzen, 1792) that did not involve intrusion in the destabilised edifice seem to have been preceded by relatively rapid flank deformation (Siebert et al., 1987). In such scenarios, geometric and qualitative kinematic (i.e. sequence of events) criteria can also be found in analogue models through detailed

photogrammetric analysis and provide invaluable constraints on the internal processes.

Extension of the results to natural volcanoes displaying incipient bulging of one flank, like Casita, may help field scientists focus their monitoring on more specific areas (the bulge crest in our case) that could give decisive information and may help recognise the operating deformation process. The latter aspect may have a fundamental importance in terms of hazard assessment because the presence of magma may greatly enhance the explosive capability in case of sector collapse of the weakened flank. Moreover, this technique enables the user to link the surface displacements to internal deformation features, as these can be inferred from model cross-sections. This method has given good results for scaled models of the 1980 Mount St. Helens cryptodome and brought geometrical and kinematic constraints on the intrusion (Donnadieu and Merle, 2001).

5. Surface photogrammetry

5.1. Experimental setting and numerical processing

This technique uses monoscopic vertical views of the models caught successively by a camera from the same position. The time frame chosen for the photograph sequence depends upon the strain rate of the models, and it is useful to have an automatic programme to take pictures at regular time intervals. The camera is maintained in a stable position above the model so that the camera focal axis is normal to the plane in which displacements are to be viewed. In our experiments, this plane view was horizontal so that the camera's focal axis was set vertically in order to avoid additional corrections during processing.

The images need to be digitised so that they can be correlated by a numerical automatic process. To this extent, a digital camera may be used instead of a classical camera but the device resolution must be the deciding factor. We used a system of two analogue Minolta Dinax 700si cameras with 50 mm focal length positioned 70 cm vertically above the model base. They were aligned along the film axis at a distance of 22 cm, i.e. the maximum horizontal interval for which the entire model was seen on both cameras. Focus was achieved at mid-height of the cone, the aperture was set to 1/22 and the exposure time to 2 s. These conditions lead to a pixel resolution of 0.15 mm with an Ektachrome Tunstene film 100 ISO. Successive images from the camera located on the side of the model with maximum deformation were used for time-differential monoscopic analysis. The accuracy of all computations depends upon the quality of the correlation programme. As processing of monoscopic views implies comparison of each smallest area (pixel) of successive pictures of the same object, zones where 'new surface' is created, or where surface area has disappeared, cannot be recognised. For example, if deep material is brought up to the surface of the model, or if part of the model surface tumbles down, or if cracks are opened up at the surface, then corresponding zones are not going to be correlated. In the case of crack or fault creation, the surface area is usually sufficiently narrow not to alter the quality of the calculated displacement picture. In a general way, the automatic correlation may fail in homogeneous zones without texture or sufficient contrast.

The topographic effect has to be removed from displacement calculations as these might be altered in magnitude (by up to 13% in our models) and orientation. The higher the point elevation, the larger the effect on displacement computations. Obviously, flat models without significant relief variations do not require such topographic corrections. For 'true 3-D' models, the parallax effect can be removed from computed displacements in two ways: (1) if two cameras are used synchronously, successive ortho-images can be built from elevations calculated with corresponding DEMs; (2) displacements calculated from original images can be corrected with a programme that takes into account a simple elevation function describing the approximate shape of the model. The second method has been used because the broad initial topography of the models was simple (a cone) and because subsequent elevation changes during each run were conspicuously an order of magnitude less than the model height.

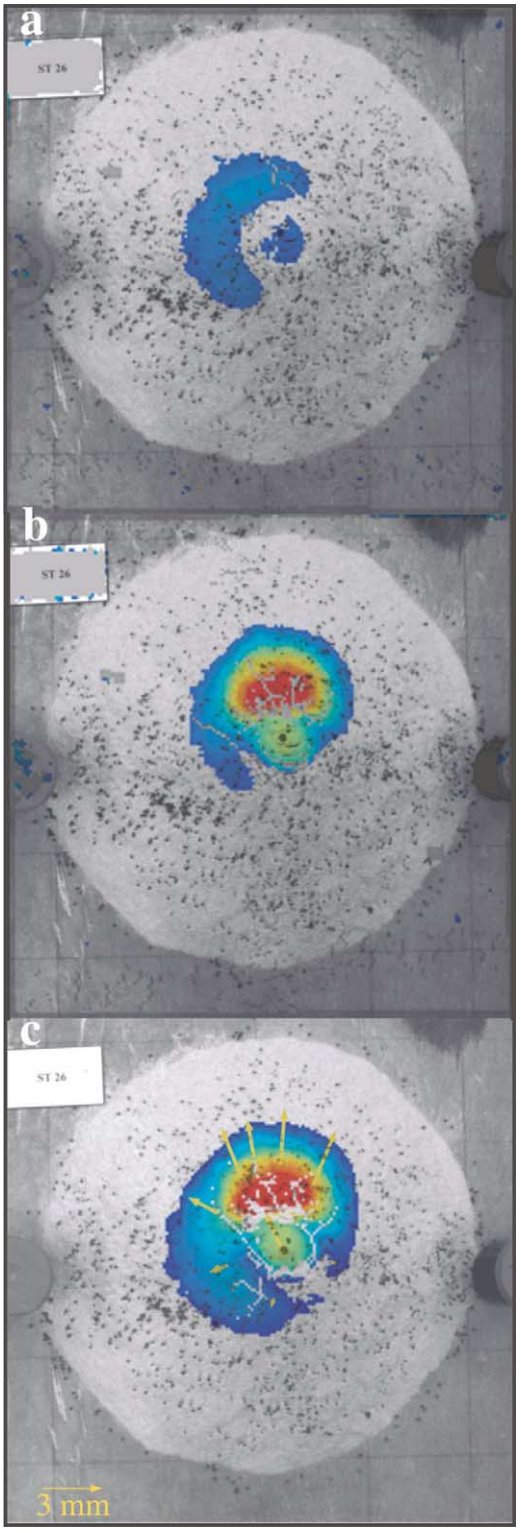

Thus, their effect was minor with respect to the topographic effect and could be discarded. Although this method might not be applicable to all kinds of models, it is more accurate and less time-consuming than ortho-image computations as it implies no DEM processing. Moreover, it requires only one camera and thus simplifies the experimental setting. Therefore, this method may display its full efficiency if used in routine experiments to observe small displacements. A programme was also added to the processing routine to remove the non-random noise stemming from imperfections of the experimental conditions (camera lenses, focus, scan etc.).

Observed displacements are a projection of the real 3-D displacements onto the camera film plane so that displacements parallel to this plane are particularly well displayed. Displacement vectors of a few selected points can be calculated from their coordinates on both images and added to the displacement magnitude picture.

5.2. Example from intrusion models

A detailed photogrammetric analysis has been conducted on the scaled intrusion models of Donnadieu and Merle (1998). It reveals radial initial displacements in a crescent-shaped area around the summit (Fig. 3a), although a whole crown sometimes forms. The magnitude of the displacements is so small (0.15–0.25 mm) that they are not visible to the naked eye in the models, corresponding to less than 5 m at the scale of an edifice like Mount St. Helens. Revealing very small displacements is a major interest of this technique, especially when they occur early in the deformation process, because they may provide an indica-

Fig. 3. Displacement maps calculated by digital photogrammetry from successive monoscopic images of an intrusion experiment. The parallax distortion is removed from computed displacements. Silicone is injected vertically into a cone at 10.7 cm/h through a conduit with diameter 0.4 cm, at a depth of 5 cm. Displacements in dark blue ≥ 0.15 mm; red ≥ 3.3 mm; light grey areas were not correlated. (a) Initial displacements after 2 h for an injected volume $V = 2.68$ cm^3; (b) displacements during following injection stage for same injection time and volume; (c) map of cumulative displacements and vectors after 4 h and $V = 5.36$ cm^3.

Table 1
Parameters and scaling ratios for intrusion model (Fig. 3) and Mount St. Helens

	Model (ST26; Fig. 3)	Mount St. Helens, 1980 (March 20 to May 16)	Ratio (MSH/model)
Intrusion viscosity (Pa s)	10^4	10^{11}	$\mu^* = 10^7$
Injection rate (m^3/h)	1.345×10^{-6}	8.2×10^4	$Q^* = 6.1 \times 10^{10}$
Injection depth (m)	0.048	1200	$h^* = 25\,000$
Cone density (kg/m^3)	1375	2200	$\rho^* = 1.6$
Gravity (m/s^2)	9.8	9.8	$g^* = 1$
Stress ratio			$\sigma^* = 40\,000$ ($= \rho^* \times g^* \times h^*$)
Time			$t^* = 250$ ($= \mu^*/\sigma^* = h^{*3}/Q^*$)
total deformation time	5.57 h	58 days	
time of Fig. 3c	4 h	42 days (i.e. May 1)	
Displacement rate			$v^* = 100$ ($= h^*/t^*$)
at bulge centre	0.78 mm/h	1.87 m/day (Goat Rock)	

tion of future fault location and may display switches in location of the active zone. Both features can be anticipated by comparison with Fig. 3b. For example, slightly longer displacements occur in the upper left part of the picture where the trace of the major shear fault separating the bulge and graben areas appears later on. Also, we observe an unexpected switch of the initial displacement location from westward (left on Fig. 3a) to clearly northward at a later stage (Fig. 3b). Another useful aspect of the technique is that calculated displacement maps show changes all over the picture area, and therefore the full extent of the deformed area. For instance, it has been shown that the bulge boundary downslope becomes clear only at the very end of the experiments as the bulge becomes completely bordered by the major shear fault (Merle and Donnadieu, 2000); in contrast, the photogrammetric analysis displays the extent of the bulge area while the shear fault tips are still propagating downhill and well before they merge and form a thrust fault at the base of the bulge. The graben and bulge structures are clearly displayed by two areas with different displacement patterns. The north and south graben contours are sharp, reflecting the structural action of the major shear fault and normal fault, respectively, and the displacement magnitude is less than in the bulge area because the downward component is more important (Fig. 3b). The bulge area is hemispherical and shows large divergent displacements decreasing downslope and appears similar to the deformation pattern of Mount St. Helens during the cryptodome intrusion in 1980 (Figs. 2b and 3b). Table 1 gives parameters of the models (Donnadieu and Merle, 1998, 2001) and those measured during the intrusive episode of Mount St. Helens in March–May 1980 (Moore and Albee, 1981; Jordan and Kieffer, 1981; Lipman et al., 1981; Alidibirov and Dingwell, 1996). For example, Jordan and Kieffer (1981) found an average steady displacement rate of 1.87 m/day between April 11 and May 12, 1980 in the Goat Rock area, i.e. the bulge centre, corresponding to displacements of about 60 m. Scaling ratios (Table 1) indicate that these values should scale down to a rate of 0.75 mm/h and displacements of 3.12 mm after 4 h in the model bulge centre, which is in very good agreement with what can be inferred from Fig. 3c. Accumulated displacements in Fig. 3c show the initial crescent-shaped area, which has spread significantly, suggesting that shearing occurs along the lower sides of the intrusion as well. Surface displacement vectors in this area are small and indicate an outward radial direction (Fig. 3c). Pictures reveal no displacement outside these areas over the rest of the cone surface. We argue that such displacements of the upper south flank (i.e. opposite to the bulge) might have existed in the early stages of deformation at Mount St. Helens. They might have remained undetected in the photogrammetric records (Moore and Albee, 1981; Jordan and Kieffer, 1981) because displacements of less than 5 m were within the technique's uncertainty and more accurate geodetic measure-

ments started too late (Lipman et al., 1981). We further argue that these small displacements of the upper south flank induced diffuse normal shearing along a zone dipping inward towards the intrusion side and that mechanical weakening of this zone contributed to the final location of the head scarp of the May 18, 1980 avalanche scar. Not coincidentally, the elongate ovoid shape of the deformation area in the models is reminiscent of the avalanche scar at Mount St. Helens.

6. Stereo-photogrammetry

The stereo-photogrammetric techniques are the most commonly used in aerial photography-based mapping and so provide results most closely comparable to those used for real volcanoes. For example, Jordan and Kieffer (1981) made a topographic map of Mount St. Helens from aerial photographs made on August 5, 1972, with scale 1:10 000 and contour interval 10 m. They also used terrain-difference models to quantitatively determine topographic changes between March and mid-May 1980. Recently, Yamashina et al. (1999) applied time-differential stereoscopy to the lava dome of Mount Unzen. They detected accelerated movement of a lava block prior to its collapse and resulting pyroclastic flow, and they studied the growth rate of a spine and its correlation to tilt measurements. Mattioli et al. (1996) also proposed a desktop image processing and photogrammetric method for rapid volcanic hazard mapping.

6.1. Experimental setting and numerical processing

Two digital images, taken at known position and orientation, allow the production of a DEM of an analogue laboratory model. Processing of stereo-image pairs uses the autocorrelation process previously described and programmes developed by Kelfoun (1999) that compute the parallax value for each homologue point and calculate the elevation of each pixel. The elevation is calculated from both (x,y) coordinate pairs produced from the correlation process for each image pixel. The accuracy of calculated elevation in our case is better than 1 mm (Kelfoun, 1999). The accuracy of computed elevations depends upon several experimental conditions, including pixel resolution of both cameras, textural quality of object surfaces (contrast, shape of small areas), conditions of camera setting (focal axes' parallelism, focus etc.; see also Section 5.1), as well as upon the resolution chosen for the DEM computations (e.g. the correlation step). A good compromise has to be found between high resolution with high noisy signal from the correlation and lower resolution with fewer morphological details. The parallax value can be used to correct an image, then called an ortho-image, and calculated elevations can be used to compute a DEM.

The first step, once the cameras have been positioned, is to calibrate the camera by laying a grid of known points on the model table. The corrections can then be used in the processing. Once the model is set up, images are taken at two points, either by two cameras simultaneously or by rapidly swapping the position of a single camera (the latter has the greatest error, as the camera position changes by small amounts each time it is moved). Dual images taken at different time periods can be used to compute displacement maps for x,y,z movements, and changes or movement of volume.

We report two types of model as examples of this process. The first is a cone with a silicone inclusion, simulating a volcano with an altered core (cf. Section 3.2; van Wyk de Vries et al., 2000; Cecchi et al., 2001). The second is a cone standing on a ductile substratum reproducing gravitational spreading (cf. Section 3.3; Merle and Borgia, 1996), as at Concepcion (van Wyk de Vries and Borgia, 1996) or Etna (Borgia et al., 1992) volcanoes.

6.2. Example from models of volcanic spreading

6.2.1. Cone with altered core

This is a similar model to that used to describe profile measurements. The advantage here is the 3-D characterisation of the whole deformation area. The images presented in Fig. 4 show the cone once it has been left to deform for 10 min and has already suffered significant movement.

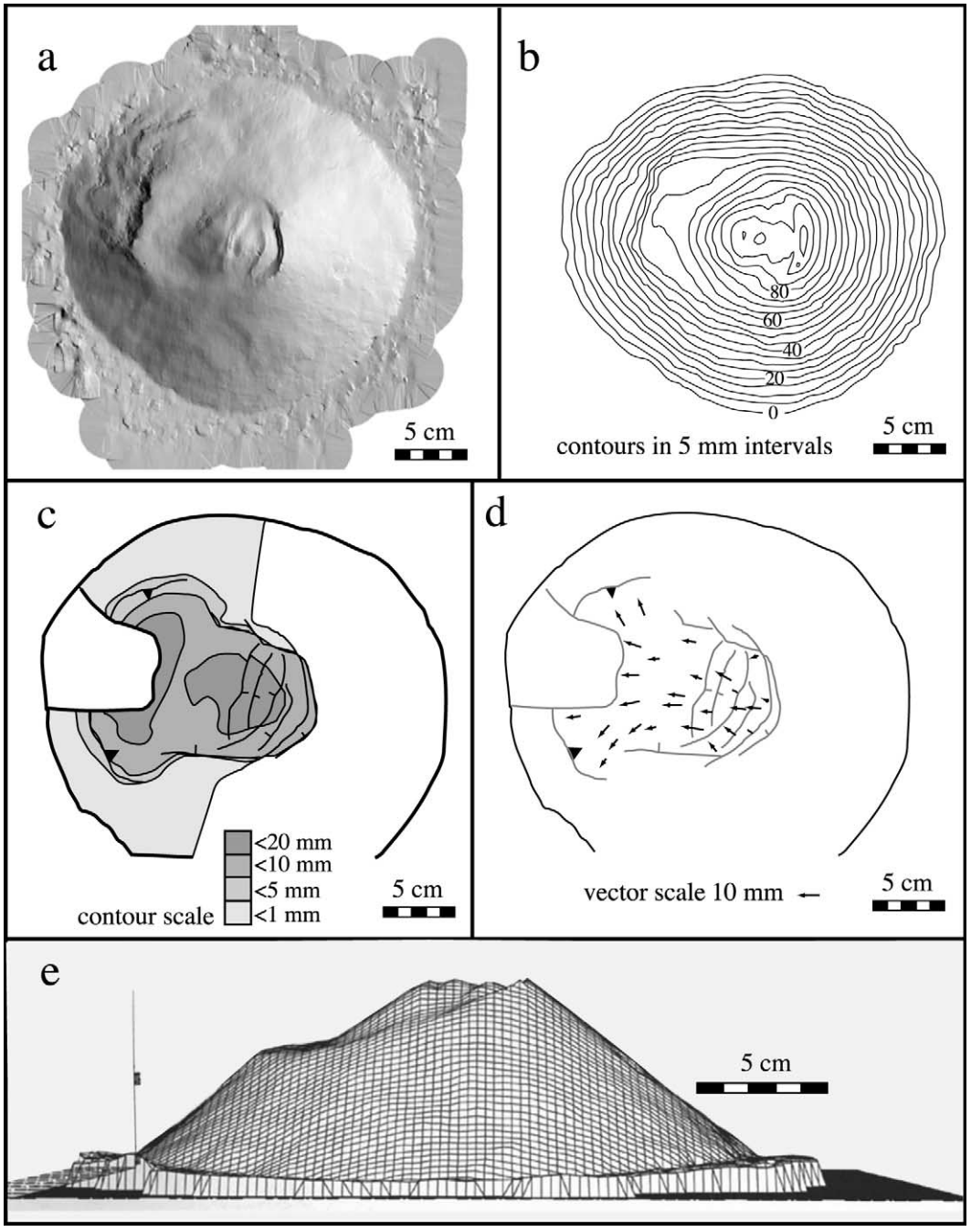

Fig. 4. Images of a stereophotographic reconstruction of a flank-spreading experiment where a weak core of silicone is used. Deformation data are obtained by comparing images taken at the start and after 10 min (10 000 years when scaled). (a) Shaded image map from deformed DEM showing the faulting. (b) Contour map of the deformed volcano. (c) Map of the vertical deformation distribution. (d) Sketch showing the fault pattern and the horizontal deformation vectors. (e) Wire-frame reconstruction of deformed cone (highest point: 9 cm above base; initial height 10 cm).

The shaded image (Fig. 4a) and the contour map (Fig. 4b) show the general form of the deformed cone. One side is undeformed and has semi-circular concentric contours. The other side is elongated in the main direction of deformation. The summit has lost its original conical shape and a flat area has appeared further down, above a steep 'bulge'. The flank oversteepening has produced a landslide, the scar of which is clearly seen. A structural map obtained from comparison of two successive ortho-images with deformation vectors and contours shows the relationship of displacement to faulting (Fig. 4c,d). Normal faults have formed at the crown of the deforming zone (Fig. 4d). These delimit the zone of deformation from the undeformed flanks. These normal faults change direction and become strike-slip faults bounding a zone of parallel deformation, which appears very different from the strongly divergent pattern of displacement vectors all over the bulge surface in the intrusion models. Further out, the deformation vectors fan out and no clear bounding fault is seen, though in other models this boundary coincides with a thrust fault.

The digital photogrammetry technique shows that small displacements occur outside the fault structures over almost half the cone surface. Vector displacements cannot be calculated for the landslide as the whole surface has been disrupted. The vertical contours show a rising area around the landslide, which corresponds to rising silicone, displaced from the mass inside the cone. This is similar, therefore, to the models with silicone intrusion, except that the bulge cross-section is wider in relation to the summit graben zone. A grid 3-D representation of the cone shows the morphologic features described above (Fig. 4e). Here the form of the deforming zone, the location of the faults, and summit graben, and the flat area and bulge are clearly seen. The flat area, in particular, is very different from the sharp transition zone between the bulge and the graben observed in the vertical-intrusion experiments. A small imperfection in the correction procedure can be seen in the curve of the tabletop represented at the base of the cone. The use of one single camera and a slight rotation of one of the image focal axes probably caused this. The experimental conditions therefore strongly control the technique's accuracy and, in particular, the ability to determine precisely absolute volume changes at the scale of these models.

6.2.2. *Spreading cone*

In the volcano spreading models of Merle and Borgia (1996), the sand cone was cohesionless and the fault pattern (leaf graben intersecting at the centre) had an overall radial symmetry. These authors have inferred radial paths for the surface particles although they describe substantial circumferential movement. There was, thus, a contradiction between assumed displacement and assumed fault slip. Our models are similar except that the cone is slightly cohesive in order to reproduce faithfully the brittle behaviour of natural rocks with a cohesive strength and to better localise strain (fault). We describe here the displacement pattern as inferred from the stereo-photogrammetry study.

The model in Fig. 5 is shown at two periods of deformation, after 10 min and after 25 min. The displacement pattern appears more complicated than previously thought, with a lot of imbricated normal faults. Major normal faults are usually curved with a strike generally approaching the radial direction and conjugate faults can be seen that form the leaf grabens described by Merle and Borgia (1996). In contrast, minor normal fault segments, not seen in sandy models but appearing clearly in our cohesive mix, are cut by major faults and show more linear trends with strikes often departing significantly from radial. For the early period, deformation vectors are roughly radial at the edge of the cone, though some vectors point into the cone and others outwards. Inside the cone, vectors are in general more circumferentially oriented, but there is a separation into areas delimited by faults. Each block has almost the same movement direction but vectors change direction and magnitude from block to block. Outside the cone, significant deformation is occurring over a wide area associated with some small thrusts, or folds verging outwards. In the 25 min image (Fig. 5b) there is a pronounced displacement field in the thrust direction. There are sharp changes on vector orientation and magnitude over

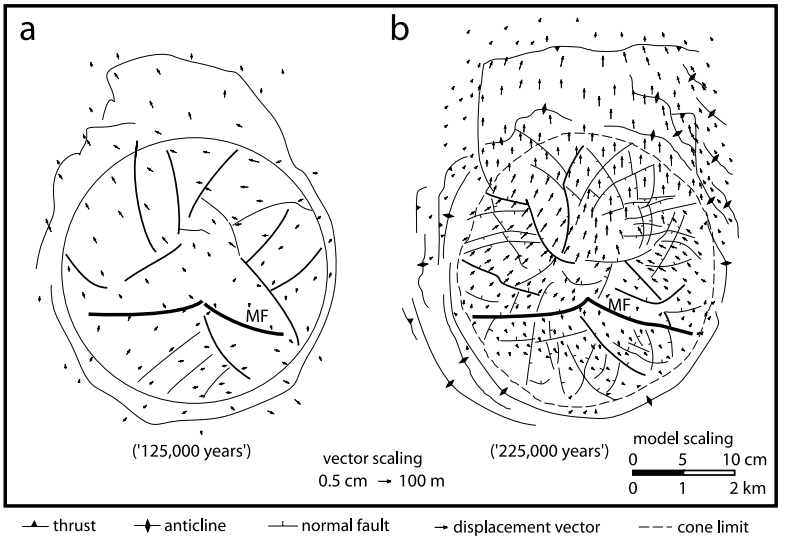

Fig. 5. Fault map of volcano spreading experiment with a cone resting on a ductile substratum (similar to Merle and Borgia, 1996). (a) Model deformation after 25 min (125 000 years in reality) and (b) after 45 min (225 000 years). While the fault pattern has previously been interpreted as being caused by radial displacement (Merle and Borgia, 1996), in both cases there is a significant departure from the radial. In panel a, while some fault-bound blocks move radially outwards, others move inwards and others tangentially. A major thrust is developing to the top of the sketch in panel a, and this direction becomes dominant in panel b, at least to one side of a major normal fault (MF). The area in the image below this fault has movement in the opposite sense.

some of the larger faults, but not over smaller ones, in contrast to earlier deformation. This suggests that blocks are deforming internally, but are still being displaced in the same general direction. The cone deformation has reached a mature stage where only a few major faults separate coherent displacement fields. Changes in displacement vector magnitude and orientation among the different displacement fields are also more conspicuous in the mature deformation regime. For instance, one major fault is clearly seen in Fig. 5b that delimits a part of the cone being displaced toward the bottom of the figure from the main field heading for the top.

A qualitative analysis of the fault pattern alone does not allow the detection of such a complicated pattern as described above. Thus the stereo-imaging allows a much more in-depth analysis of the models. The models can be used for explaining anomalous displacements and structures recorded in the field. For example GPS-measured displacements at Concepcion, Nicaragua, indicate significant non-radial movements. Using the analogue models we can now interpret these movements as spreading of the volcano along non-radial faults separated into structural blocks.

7. Discussion

The three techniques of photogrammetric analysis described here have different purposes, a different accuracy, imply different amounts of image processing, and provide different types of data. Therefore, the use of one particular method should be selected according to the specific goal of the experimental study, although several of them might be conveniently combined.

The side-perspective video technique is quick and easy to implement and provides accurate displacement trajectory data for a few selected points. This technique alone is not appropriate for the study of complicated broad deformation patterns but is very useful in analysing deformation rates and sequences of a few selected points and bringing strong clues on the deformation process. Displacement profiles can be recorded anywhere in the deformation area but, naturally, it is

useful to seek the line of largest displacements, because most deformation features will have their maximum amplitude and will be the most distinctive. In this case, the user has to have a rough idea of the displacement pattern and how this line will be oriented prior to implementing this technique. Some clues can be revealed by a surface photogrammetry analysis of early displacements or the observation of structural features at the very beginning of the deformation. In the models presented here, the main strain direction is not known a priori, so this implies waiting for the appearance of precursors of the main deformation (e.g. direction of incipient bulging, orientation of arcuate faults) and displacements at the very beginning might not be recorded. The strong interest of this method, however, is that displacement measurements are generally directly comparable with profiles obtained from geodetic surveys carried out on active volcanoes (e.g. precision or trigonometric levelling, trilateration, GPS) and can provide clues on processes occurring at depth. For example, geodetic measurements by geodimeter and theodolite on the bulge of Mount St. Helens in 1980 showed a net uplift of the northern flank and indicated intrusion of magma (Lipman et al., 1981). The advantage of using a video film rather than time-framed photographs lies in the fact that the time interval of videogram pictures can be chosen after the experimental run according to the observed model surface displacement rate, which is generally known only a posteriori. In contrast, using a video system as opposed to a digital camera provides a lower resolution, but one good enough to follow reference points and accurately study small displacements (≥ 0.1 mm). Obviously, this method could also be used with vertical photographs to get horizontal displacement trajectories of specific points of the model's top surface.

For broad displacement patterns, a photogrammetric analysis of the whole surface area by numerical correlation is found to be more convenient because it gives results for each pixel area. Photogrammetry from monoscopic views enables the user to detect very small displacements over wide areas that may help to anticipate fault location and switching of active zones, as well as to interpret model deformation. This method requires a less complicated experimental setting and less numerical processing than stereo-photogrammetry. Hence, there is a smaller displacement detection threshold. This method is, thus, better when tiny displacements are sought, when the initial topography can be modelled by a simple function, when the displacements are small with regard to the elevation and, finally, when they occur mainly in the plane normal to the focal axis. On real volcanoes, photogrammetric analysis from aerial photographs and InSAR surveys, as well as data from extensive arrays of geodetic points, would give results comparable to those obtained in the experiments by monoscopic and stereo-photogrammetry. For instance, a very good agreement was found between results from the scaled intrusion models presented and deformation measurements by digital photogrammetry made during the bulging episode of the north flank of Mount St. Helens in 1980 (Moore and Albee, 1981; Jordan and Kieffer, 1981).

The stereo-photogrammetric method is the most powerful of the three techniques presented, as most information can be inferred from DEMs, or ortho-images, for each point of the picture, such as elevation changes, displacement maps or vectors. In contrast, it is the most time-consuming method in terms of setting the experimental conditions to a satisfying degree of accuracy, and numerical processing. Large storage capacity is also required for computed files. The detection threshold is higher than that of monoscopic photogrammetry as more numerical processing is involved and problems often arise to calculate accurately volume changes. Airborne stereoscopic photogrammetry is a powerful tool to derive high-resolution DEMs on dangerous and inaccessible areas such as volcanoes. Also, methods like n-view reconstruction and its recent applications in volcanology for morphological modelling and deformation measurement (Cecchi et al., 2003), or airborne laser swath mapping (Carter et al., 2001) seem very promising. However, although time-differential stereoscopy or InSAR data are potentially very useful to detect volcano deformation, these techniques are limited by the accuracy achievable. The accuracy of the digital photo-

grammetry technique applied to volcanoes is limited, for example, by the presence of vegetation, shadowing effects, morphology, scale of the images, and efficiency of the image matching procedure. The accuracy of the InSAR technique is also limited by the presence of vegetation and the time interval between two consecutive sets of data, i.e. orbit parameters of the satellite.

8. Conclusions

We have shown that digital photogrammetry in a broad sense is a useful tool in analogue modelling in general. It provides quantitative spatio-temporal data on model surface displacements that come in addition to qualitative information from classical observation. The interest of the experimental techniques presented here is two-fold. First, detailed photogrammetric analysis of scaled analogue models may enable volcanologists to obtain clues about the deformation process. This is of importance because the nature of deformation processes (e.g. presence of magma, volume, injection rate, direction and size of potential collapse) has direct implications for volcano hazards, particularly hazards associated with flank instability. Secondly, the experimental techniques are directly comparable to most monitoring techniques of real volcanoes.

Images retrieved from side-perspective videos give displacement profiles of selected points. These can be compared with data obtained in the field by geodetic monotoring (levelling, trilateration, GPS). For example, geodimeter and theodolite measurements made on the bulge of Mount St. Helens in March–May 1980 enabled volcanologists to infer a magmatic intrusion in the northern flank. Data from extensive arrays of geodetic points, aerial photograph analysis, or InSAR surveys would give results more comparable to the other techniques, monoscopic and stereo-photogrammetry respectively. Thus, direct and quantitative comparison between scaled models and natural volcanoes can be made, as illustrated by scaled intrusion models and photogrammetric surveys at Mount St. Helens. Models can be used to determine the most useful sites for monitoring, by finding areas of maximum anticipated displacement. Conversely, hypotheses about the origin of deformation can be rapidly checked with analogue models. For example, profile measurements using a camera linked to the web could provide near real-time measurements on the growth of a dome or bulge. These data could be interpreted by models running concurrently with data acquisition.

Improvement of the technique's accuracy and adaptability in the field, especially for DEMs, has the potential to create a highly valuable tool for hazard assessment.

Acknowledgements

We acknowledge P. Baldi and S.J. Day for constructive reviews. This work has been funded by the French P.N.R.N. project RV03.

References

Acocella, V., Cifelli, F., Funiciello, R., 2000. Analogue models of collapse calderas and resurgent domes. J. Volcanol. Geotherm. Res. 104, 81–96.

Alidibirov, M., Dingwell, D.B., 1996. Magma fragmentation by rapid decompression. Nature 380, 146–148.

Baldi, P., Bonvalot, S., Briole, P., Marsella, M., 2000. Digital photogrammetry and kinematic GPS applied to the monitoring of Vulcano Island, Aeolian Arc. Ital. Geophys. J. Int. 142, 801–811.

Begét, J.E., Kienle, J., 1992. Cyclic formation of debris avalanches at Mt. St. Augustine volcano, Alaska. Nature 356, 701–704.

Benn, K., Odonne, F., de Saint Blanquat, M., 1998. Pluton emplacement during transpression in brittle crust; new views from analogue experiments. Geology 26, 1079–1082.

Blake, S., 1990. Viscoplastic models of lava domes. In: Fink, J.H. (Ed.), Lava Flows and Domes - Emplacement Mechanisms and Hazard Implications, IAVCEI Proc. Volcanol., vol. 2. Springer, pp. 88–126.

Borgia, A., 1994. Dynamic basis of volcanic spreading. J. Geophys. Res. 99, 17791–17804.

Borgia, A., Delaney, P.T., Denlinger, R.P., 2000. Spreading volcanoes. Annu. Rev. Earth Planet. Sci. 28, 539–570.

Borgia, A., Ferrari, L., Pasquare, G., 1992. Importance of gravitational spreading in the tectonic and volcanic evolution of Mount Etna. Nature 357, 231–235.

Carracedo, J.-C., 1994. The Canary Islands: an example of structural control on the growth of large oceanic-island volcanoes. J. Volcanol. Geotherm. Res. 60, 225–241.

Carter, W., Shrestha, R., Tuell, G., Bloomquist, D., Sartori, M., 2001. Airborne laser swath mapping shines new light on Earth's topography. EOS Trans. AGU 82, 549–555.

Cecchi, E., Van Wyk de Vries, B., Garaebiti, E., 2001. Numerical and analogue modelling of volcano flank spreading: characterisation of structure, morphology and associated landslide activity. E.U.G. XI Gen. Ass., Strasbourg, p. 85.

Cecchi, E., van Wyk de Vries, B., Lavest, J.-M., Harris, A., Davies, M., 2003. N-view reconstruction: a new method for morphological modelling and deformation measurement in volcanology. J. Volcanol. Geotherm. Res. 123, 181–201.

Cloos, H., 1928. Experimente zur inneren Tektonic. Zent.bl. Mineral. Paläontol. 1928, 609–621.

Day, S.J., 1996. Hydrothermal pore fluid pressure and the stability of porous, permeable volcanoes. In: McGuire, W.J., Jones, A.P., Neuberg, J. (Eds.), Volcano Instability on the Earth and Other Planets. Geol. Soc. Lond. Spec. Publ. 110, pp. 77–93.

Donnadieu, F., Merle, O., 1998. Experiments on the indentation process during cryptodome intrusions: new insights into Mount St. Helens deformation. Geology 26, 79–82.

Donnadieu, F., Merle, O., 2001. Geometrical constraints of the 1980 Mount St. Helens intrusion from analogue models. Geophys. Res. Lett. 28, 639–642.

Donnadieu, F., Merle, O., Besson, J.-C., 2001. Volcanic edifice stability during cryptodome intrusion. Bull. Volcanol. 63, 63–72.

Elsworth, D., Voight, B., 1995. Dike intrusion as a trigger for large earthquakes and failure of volcano flanks. J. Geophys. Res. 100, 6005–6024.

Elsworth, D., Voight, B., 1996. Evaluation of volcano flank instability triggered by dyke intrusion. In: McGuire, W.J., Jones, A.P., Neuberg, J. (Eds.), Volcano Instability on the Earth and Other Planets. Geol. Soc. Lond. Spec. Publ. 110, pp. 45–53.

Fink, J.H., Griffiths, R.W., 1990. Radial spreading of viscous-gravity currents with solidifying crust. J. Fluid Mech. 221, 485–509.

Fink, J.H., Griffiths, R.W., 1998. Morphology, eruption rates, and rheology of lava domes: insights from laboratory models. J. Geophys. Res. 103, 527–545.

Fink, J.H., Malin, M.C., Anderson, S.W., 1990. Intrusive and extrusive growth of the Mount St. Helens lava dome. Nature 348, 435–437.

Firth, C., Stewart, I., McGuire, W.J., Kershaw, S., Vita-Finzi, C., 1996. Coastal elevation changes in eastern Sicily: implications for volcano instability at Mount Etna. In: McGuire, W.J., Jones, A.P., Neuberg, J. (Eds.), Volcano Instability on the Earth and Other Planets. Geol. Soc. Lond. Spec. Publ. 110, pp. 153–167.

Fiske, R.S., Jackson, E.D., 1972. Orientation and growth of Hawaiian volcanic rifts: the effect of regional structure and gravitational stresses. Proc. R. Soc. London 329, 299–326.

Francis, P.W., Self, S., 1987. Collapsing volcanoes. Sci. Am. 255, 90–97.

Gorshkov, G.S., 1959. Gigantic eruption of the volcano Bezymianny. Bull. Volcanol. 20, 77–109.

Gruen, A.W., 1985. Adaptative least squares correlation: a powerful image matching technique. S. Afr. J. Photogram. Rem. Sens. Cart. 14, 175–187.

Guest, J.E., Duncan, A.M., Chester, D.K., 1988. Monte Vulture volcano (Basilicata, Italy): an analysis of morphology and volcaniclastic facies. Bull. Volcanol. 50, 244–257.

Head, J.W.I., 1996. Volcano instability development: a planetary perspective. In: McGuire, W.J., Jones, A.P., Neuberg, J. (Eds.), Volcano Instability on the Earth and Other Planets. Geol. Soc. Lond. Spec. Publ. 110, pp. 5–43.

Howe, E., 1901. Experiments illustrating intrusion and erosion. U.S. Geol. Surv. 21st Ann. Rep. 3, pp. 291–303.

Hubbert, M.K., 1937. Theory of scale models as applied to the study of geologic structures. Geol. Soc. Am. Bull. 48, 1459–1520.

Jordan, R., Kieffer, H.H., 1981. Topographic changes at Mount St. Helens: large-scale photogrammetry and digital terrain models. In: Lipman, P.W., Mullineaux, D.R. (Eds.), The 1980 Eruptions of Mount St. Helens, Washington. U.S. Geol. Surv. Prof. Pap. 1250, pp. 135–141.

Kanamori, H., Given, J.W., Lay, T., 1984. Analysis of seismic body waves excited by the Mount St. Helens eruption of May 18, 1980. J. Geophys. Res. 89, 1856–1866.

Katsui, Y., Komuro, H., Uda, T., 1985. Development of faults and growth of Usu-Shinzan cryptodome in 1977-1982 at Usu volcano, north Japan. J. Fac. Sci. Hokkaido Univ. Serie IV 21, 339–362.

Kelfoun, K., 1999. Processus de croissance et déstabilisation des dômes de lave du Merapi (Java Centrale, Indonésie): modélisations numériques des dômes, dynamique des écoulements pyroclastiques associés et surveillance par stéréo-photogrammétrie. Ph.D. Thesis, Univ. Clermont-Ferrand II, France, 261 pp.

Kerle, N., van Wyk de Vries, B., 2001. The 1998 debris avalanche at Casita volcano, Nicaragua - investigation of structural deformation as the cause of slope instability using remote sensing. J. Volcanol. Geotherm. Res. 105, 49–63.

Komuro, H., 1987. Experiments on cauldron formation: a polygonal cauldron and ring fractures. J. Volcanol. Geotherm. Res. 31, 139–149.

Komuro, H., Fujita, Y., Kodama, K., 1984. Numerical and experimental models on the formation mechanism of collapse basins during the Green tuff orogenesis of Japan. Bull. Volcanol. 47, 649–666.

Lagabrielle, Y., Garel, E., Dauteuil, O., Cormier, M.-H., 2001. Extensional faulting and caldera collapse in the axial region of fast spreading ridges: analog modeling. J. Geophys. Res. 106, 2005–2015.

Lagmay, A.M.F., van Wyk de Vries, B., Kerle, N., Pyle, D.M., 2000. Volcano instability induced by strike-slip faulting. Bull. Volcanol. 62, 331–346.

Lipman, P.W., Moore, J.G., Swanson, D.A., 1981. Bulging of the north flank before the May 18 eruption - geodetic data. In: Lipman, P.W., Mullineaux, D.R. (Eds.), The 1980 Eruptions of Mount St. Helens, Washington. U.S. Geol. Surv. Prof. Pap. 1250, pp. 143–155.

Lopez, D.L., Williams, S.N., 1993. Catastrophic volcanic col-

lapse: relation to hydrothermal processes. Science 260, 1794–1796.

Maciejak, F., 1998. Apport du traitement d'image, de la stéréo-photogrammétrie numérique et de la morphologie par les ombres à l'étude du volcanisme martien. Application à Tharsis Tholus, Ceraunius Tholus, Uranius Tholus et Uranius Patera. Ph.D. Thesis, Univ. Clermont-Ferrand II, France, 315 pp.

Martí, J., Ablay, G.J., Redshaw, L.T., Sparks, R.S.J., 1994. Experimental studies of collapse calderas. J. Geol. Soc. Lond. 151, 919–929.

Mattioli, G.S., Jansma, P.E., Jaramillo, L., Smith, A.L., 1996. A desktop image processing and photogrammetric method for rapid volcanic hazard mapping: application to air-photo interpretation of Mount Pélée, Martinique. Bull. Volcanol. 58, 401–410.

McClay, K.R., 1996. Recent advances in analogue modelling: uses in section interpretation and validation. In: Buchanan, P.G., Nieuwland, D.A. (Eds.), Modern Developments in Structural Interpretation, Validation and Modelling. Geol. Soc. Lond. Spec. Publ. 99, pp. 201–225.

McGuire, W.J., 1996. Volcano instability: a review of contemporary themes. In: McGuire, W.J., Jones, A.P., Neuberg, J. (Eds.), Volcano Instability on the Earth and Other Planets. Geol. Soc. Lond. Spec. Publ. 110, pp. 1–23.

Merle, O., Borgia, A., 1996. Scaled experiments of volcanic spreading. J. Geophys. Res. 101, 13805–13817.

Merle, O., Donnadieu, F., 2000. Indentation of volcanic edifices by the ascending magma. In: Vendeville, B., Mart, Y., Vigneresse, J.-L. (Eds.), Salt, Shale and Igneous Diapirs in and around Europe. Geol. Soc. Lond. Spec. Publ. 174, pp. 43–53.

Merle, O., Vendeville, B., 1995. Experimental modelling of thin-skinned shortening around magmatic intrusions. Bull. Volcanol. 57, 33–43.

Merle, O., Vidal, N., Van Wyk de Vries, B., 2001. Experiments on vertical basement fault reactivation below volcanoes. J. Geophys. Res. 106, 2153–2162.

Moore, J.G., Albee, W.C., 1981. Topographic and structural changes, March-July 1980 - photogrammetric data. In: Lipman, P.W., Mullineaux, D.R. (Eds.), The 1980 Eruptions of Mount St. Helens, Washington. U.S. Geol. Surv. Prof. Pap. 1250, pp. 123–134.

Moore, J.G., Clague, D.A., 1992. Volcano growth and evolution of the island of Hawaii. Geol. Soc. Am. Bull. 104, 1471–1484.

Murray, J.B., 1988. The influence of loading by lavas on the siting of volcanic eruption vents on Mt. Etna. J. Volcanol. Geotherm. Res. 35, 121–139.

Otto, G.P., Chau, T.K.W., 1989. Region-growing algorithm for matching of terrain images. Image Vis. Comput. 7, 2.

Pollard, D.D., Johnson, A.M., 1973. Mechanics of growth of some laccolithic intrusions in the Henry Mountains, Utah - II. Bending and failure of overburden layers and sill formation. Tectonophysics 18, 311–354.

Ramberg, H., 1970. Model studies in relation to intrusion of plutonic bodies. In: Newall, G., Rast., N. (Eds.), Mechanism of Igneous Intrusion. Geol. J. Spec. Iss. 2, pp. 261–286.

Ramberg, H., 1981. Gravity, Deformation and the Earth's Crust in Theory, Experiments and Geological Applications. Academic Press, London, 214 pp.

Roche, O., Druitt, T.H., Merle, O., 2000. Experimental study of caldera formation. J. Geophys. Res. 105, 395–416.

Roman-Berdiel, T., Gapais, D., Brun, J.P., 1995. Analogue models of laccolith formation. J. Struct. Geol. 17, 1337–1346.

Roman-Berdiel, T., Gapais, D., Brun, J.P., 1997. Granite intrusion along strike-slip zones in experiment and nature. Am. J. Sci. 297, 651–678.

Siebert, L., 1984. Large volcanic debris avalanches: characteristics of source areas, deposits, and associated eruptions. J. Volcanol. Geotherm. Res. 22, 163–197.

Siebert, L., Glicken, H., Ui, T., 1987. Volcanic hazards from Bezymianny- and Bandaï-type eruptions. Bull. Volcanol. 49, 435–459.

Tibaldi, A., 1995. Morphology of pyroclastic cones and tectonics. J. Geophys. Res. B 100, 24521–24535.

van Wyk de Vries, B., Francis, P.W., 1997. Catastrophic collapse at stratovolcanoes induced by slow volcano spreading. Nature 387, 387–390.

van Wyk de Vries, B., Borgia, A., 1996. The role of basement in volcano deformation. In: McGuire, W.J., Jones, A.P., Neuberg, J. (Eds.), Volcano Instability on the Earth and Other Planets. Geol. Soc. Lond. Spec. Publ. 110, pp. 95–110.

van Wyk de Vries, B., Kerle, N., Petley, D., 2000. Sector collapse forming at Casita volcano, Nicaragua. Geology 28, 167–170.

van Wyk de Vries, B., Matela, R., 1998. Styles of volcano-induced deformation: numerical models of substratum flexure, spreading and extrusion. J. Volcanol. Geotherm. Res. 81, 1–18.

van Wyk de Vries, B., Merle, O., 1996. The effect of volcanic constructs on rift fault patterns. Geology 24, 643–646.

van Wyk de Vries, B., Merle, O., 1998. Extension induced by volcanic loading in regional strike-slip zones. Geology 26, 983–986.

Vidal, N., Merle, O., 2000. Reactivation of basement faults beneath volcanoes; a new model of flank collapse. J. Volcanol. Geotherm. Res. 99, 9–26.

Voight, B., 1988. A method for prediction of volcanic eruptions. Nature 332, 125–130.

Voight, B., 2000. Structural stability of andesite volcanoes and lava domes. In: Francis, P.W., Neuberg, J., Sparks, R.S.J. (Eds.), Causes and Consequences of Eruption of Andesite Volcanoes. Philos. Trans. R. Soc. 358, pp. 1663–1703.

Voight, B., Elsworth, D., 1997. Failure of volcano slopes. Géotechnique 47, 1–31.

Voight, B., Glicken, H., Janda, R.J., Douglass, P.M., 1981. Catastrophic rockslide avalanche of May 18. In: Lipman, P.W., Mullineaux, D.R. (Eds.), The 1980 Eruptions of Mount St. Helens, Washington. U.S. Geol. Surv. Prof. Pap. 1250, pp. 347–377.

Weber, D., Hermann, A., 2000. Contribution de la photo-

grammétrie numérique à l'étude spatio-temporelle de versants instables: l'exemple du glissement de terrain de Super-Sauze (Alpes-de-Haute-Provence, France). Bull. Soc. Géol. France 171, 637–648.

Weijermars, R., Jackson, M.P.A., Vendeville, B., 1993. Rheological and tectonic modeling of salt provinces. Tectonophysics 217, 143–174.

Yamashina, K., Matsushima, T., Ohmi, S., 1999. Volcanic deformation at Unzen, Japan, visualized by a time-differential stereoscopy. J. Volcanol. Geotherm. Res. 89, 73–80.

Zlotnicki, J., Ruegg, J.C., Bachelery, P., Blum, P.A., 1990. Eruptive mechanism on Piton de la Fournaise volcano associated with the December 4, 1983, and January 18, 1984 eruptions from ground deformation monitoring and photogrammetric surveys. J. Volcanol. Geotherm. Res. 40, 197–217.